View metadata, citation and similar papers at core.ac.uk
brought to you by CORE
provided by University of Essex Research Repository

Microstrip Device for Broadband (15–65 GHz) Measurement of Dielectric Properties of Nematic Liquid Crystals

Prafulla Deo, *Member, IEEE*, Dariush Mirshekar-Syahkal, *Fellow, IEEE*, Lawrence Seddon, Sally E. Day, *Member, IEEE*, and F. Aníbal Fernández, *Member, IEEE*

***Abstract*—The essential dielectric properties, the basic alignment techniques, and the common measurement methods of the nematic liquid crystal (LC) at RF are briefly reviewed. A new device for the broadband measurement of the dielectric constants and loss tangents of nematic LCs at microwave and millimeter-wave frequencies is presented. This device whose specification and fabrication are outlined is essentially a two dielectric layer microstrip structure with coplanar-waveguide terminals, which is easy to fabricate. Compared to previous structures, the proposed device is extremely broadband with 15–65-GHz bandwidth, benefits from a solid exposed ground plane for easy temperature test, and operates under bias voltage. The technique for the extraction of the dielectric parameters of the nematic LC analyzed by this device is explained and the sources imposing the frequency limits on the device performance are identified. Two different nematic LCs, MDA-00-3506 and GT3-23001, are characterized and the results are shown to compare well with those available in the literature. In the comparisons, the maximum difference found for the dielectric constants for MDA-00-3506 is 5% and for GT3-23001 is 5.3%.**

***Index Terms*—Dielectric measurement, liquid crystals (LCs), microstrip lines, millimeter-wave tunable devices.**

I. Introduction

DUE TO its voltage tunable dielectric [1]–[3], the nematic (rod type) liquid crystal (LC) has attracted the attention of researchers in the RF field and is used to develop voltage-controlled tunable devices at microwave and millimeter-wave frequencies [4]. Some of the LC-based devices investigated so far include variable phase shifters, tunable patch antennas, reflect arrays, beam-steering antennas, and tunable resonators and filters [5]–[13].

Manuscript received October 07, 2014; revised December 12, 2014 and January 20, 2015; accepted February 06, 2015. This work was supported by the Engineering and Physical Sciences Research Council (EPSRC), U.K.

P. Deo was with the School of Computer Science and Electronic Engineering, University of Essex, Colchester CO4 3SQ, U.K. He is now with the Jodrell Bank Centre of Astrophysics, School of Physics and Astronomy, The University of Manchester, Manchester M13 9PL, U.K. (e-mail: prafulla.deo@manchester.ac.uk).

D. Mirshekar-Syahkal is with the School of Computer Science and Electronic Engineering, University of Essex, Colchester CO4 3SQ, U.K.

L. Seddon, S. E. Day, and F. A. Fernández are with the Department of Electronic and Electrical Engineering, University College London, London WC1E 7JE, U.K.

Color versions of one or more of the figures in this paper are available online at http://ieeexplore.ieee.org.

Digital Object Identifier 10.1109/TMTT.2015.2407328

These devices use different nematic LCs, which, amongst the broad range of LCs available, have simple structures and behaviors. Nematic LCs are relatively cheap, respond to low voltages, and are highly linear under large RF fields [14]. These properties allow nematic LCs to offer various advantages over ferroelectrics and piezoelectrics [15], [16] in many RF applications in spite of their slower response time.

The molecules of the nematic LC have no positional regularity, but they possess a long-range orientational order. An order tensor is defined for the macroscopic ordering, representing the local orientation of the molecules through the director, $\hat{n}$, and the ordering degree [1]–[3]. The permittivity of nematic LCs is defined by a uniaxial second-rank tensor, $\overline{\overline{\varepsilon}}$, whose principal elements $\varepsilon_{||}$ and $\varepsilon_{\perp}$ are permittivities parallel and normal to $\hat{n}$ [3]. Therefore, if for a bias electric field at a position in the LC the unit vector $\hat{n}$ is along the x-axis, the electric flux density, $\mathbf{D}$, and the electric field, $\mathbf{E}$, at that point are related through

$$\begin{pmatrix} D_x \\ D_y \\ D_z \end{pmatrix} = \begin{pmatrix} \varepsilon_{||} & 0 & 0 \\ 0 & \varepsilon_{\perp} & 0 \\ 0 & 0 & \varepsilon_{\perp} \end{pmatrix} \begin{pmatrix} E_x \\ E_y \\ E_z \end{pmatrix}. \quad (1)$$

From (1), it is inferred that $\varepsilon_{||}$ is the permittivity for the component of $\mathbf{E}$ parallel to $\hat{n}$ and $\varepsilon_{\perp}$ is the permittivity for the component perpendicular to $\hat{n}$. These principal elements of $\overline{\overline{\varepsilon}}$ can be complex quantities accounting for dielectric losses. By changing the strength of the bias field, $\hat{n}$ rotates, the values of all the elements of $\overline{\overline{\varepsilon}}$ change and $\mathbf{D}$ varies, thus the nematic LC offers dielectric tunability.

Normally, $\varepsilon_{\perp}$ and $\varepsilon_{||}$ in (1) are functions of frequency. At dc and low frequencies they have large values, whereas at RF including microwave and millimeter-wave frequencies, they approach (smaller) constant values. The most important factors influencing the choice of an LC for a particular RF application are the dielectric anisotropy ($\Delta\varepsilon_r = \varepsilon_{r||} - \varepsilon_{r\perp}$), the dielectric losses (loss tangents $\tan(\delta_{||})$ and $\tan(\delta_{\perp})$), the switching voltage threshold, and the transition voltage [1]–[3]. The values for the anisotropy and the losses are of utmost importance as the first one directly controls the range of tunability of an LC-based device, and the second, its RF power dissipation.

The resonant and the broadband transmission line methods have been used to obtain the dielectric properties of nematic LCs at RF. Although it offers high sensitivity, the resonant method is applicable at single frequencies and it is difficult for extracting

This work is licensed under a Creative Commons Attribution 3.0 License. For more information, see http://creativecommons.org/licenses/by/3.0/

This article has been accepted for inclusion in a future issue of this journal. Content is final as presented, with the exception of pagination.

the loss tangents accurately [17]–[19]. The broadband transmission line method is normally the preferred option. Some broadband methods employ coaxial lines [20] as the test device, while others employ rectangular waveguides [21]. In [17], [20], and [21], a strong magnetic field is employed to align the LC molecules in two orthogonal directions. However, it is more practical for circuit applications to use the electric field (produced by low voltages) to bias the nematic LC, as mentioned in the resonant methods in [18] and [19].

In [22], a broadband method is proposed using a planar transmission line. One of its advantages is the control of the alignment of the LC molecules through the bias voltage directly applied to the LC under test. As in the resonant methods in [18] and [19], the method in [22] requires initial aligning of LC molecules in the test device. The alignment is achieved by appropriate treatment of boundary surfaces (mainly electrodes) of the test device so that at no bias voltage the director ($\hat{n}$) is in the direction of wave propagation, governed by the surface treatment. This default (or preferred) alignment can be realized by coating the boundary surfaces with a thin polyimide layer, followed by annealing and rubbing the layer [23]. Upon the application of an external bias voltage across electrodes, the director aligns in a direction minimizing the free energy of the system. Essentially, this induced alignment is not in the direction of the biasing field. Nevertheless, applying a sufficiently large bias voltage, the director in the bulk of the LC layer turns completely along the bias field (if $\varepsilon_{||} > \varepsilon_{\perp}$). The evaluation of the field of the director ($\hat{n}$) can be done by the free-energy expression from the Oseen–Frank theory [3], [24], which requires dc (or very low frequency) values of $\varepsilon_{||}$ and $\varepsilon_{\perp}$ represented by $\varepsilon_{||b}$ and $\varepsilon_{\perp b}$, respectively, and elastic constants K_{11}, K_{22}, and K_{33} of the LC. These parameters, normally provided by LC manufacturers, are important in the accurate and reliable design of LC-based RF devices.

The test device in [22] was demonstrated to be suitable for measuring the dielectric properties of nematic LCs from 30 to 60 GHz. However, for frequencies above 60 GHz, the device was found to be undesirable owing to its high conductor and surface wave radiation losses. The fabrication of the device is also complex as it consists of a three-layer structure with six via holes of which two are vertical vias connecting the input/output to the LC cell arranged in the form of a microstrip line. Furthermore, as the ground plane in that device is between two dielectric layers, the test for the variation of the LC parameters with temperature requires a small enclosed environment, which is difficult to achieve using a probe-station.

To alleviate the problems with the device in [22], a new test device is presented in this paper (Fig. 1). It has a 20-GHz wider band, it has a very simple structure, it can be manufactured in large volumes at low cost, and for this reason, it can be discarded after use. Also due to this property, LC laboratories that have no access to microwave/millimeter-wave measurement equipment, can fill the new test device with their LCs and send their samples to a measurement facility for characterization. The new device has a two-layer microstrip structure with exposed ground plane and via-holes to the ground only. In this device, the LC section (cell) is a fixed length suspended microstrip line embracing the LC layer for evaluation. The surfaces of the ground plane and the strip line are preconditioned, and hence, the LC molecules can be re-oriented by applying a bias voltage to the cell. Each terminal of the cell is integrated with a broadband coplanar waveguide (CPW) to microstrip-line transitions. Through any of these two identical transitions, the bias voltage can be conveniently applied using a bias tee, and when the CPWs on the device are made compatible with the CPW probe on the probe stations, the S-parameters (scattering parameters) for the LC cell can be accurately determined. The new device is simple to fabricate and since it has very thin dielectric layers and no via-holes on the main strip line, it has lower return losses as well as lower surface wave radiation losses. The proposed test device allows the evaluation of electrical parameters of nematic LCs within the broad band of 15–65 GHz.

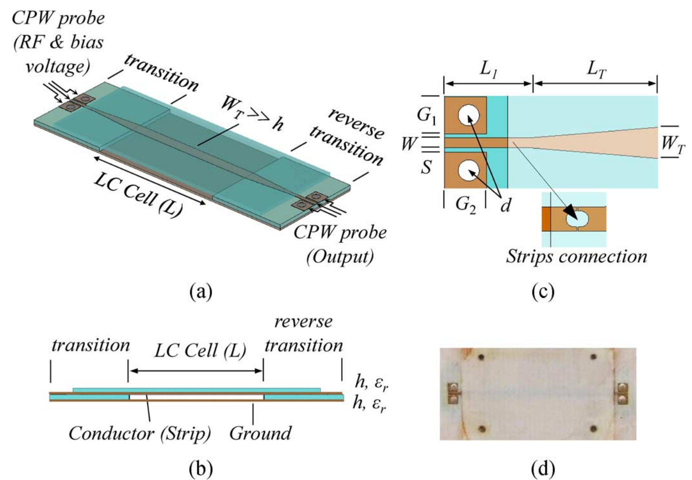

Fig. 1. LC test device. (a) Perspective view. (b) Longitudinal cross-sectional view. (c) CPW-microstrip line transition. (d) Fabricated prototype. The bias voltage is applied through one of the RF ports using a bias tee.

This paper is organized into six sections. In Section II, the structure and the parameters of the new test device are introduced. In Section III, the technique for de-embedding the effects of the CPW–microstrip transitions from the measurements is outlined and then frequency limits of the device and relevant results for comparison purposes by prospective users are presented. In Section IV, measurement results of dielectric constants and loss tangents for two nematic LCs, namely, MDA-00-3506 and GT3-23001, using the proposed test device are presented and analyzed. In Section V, an uncertainty analysis for the technique is outlined.

II. Device Structure and Parameters

The schematic of the new broadband planar LC test device for the characterization of the nematic LC is shown in Fig. 1. It comprises the LC cell formed between the conducting strip and the ground plane of the suspended microstrip line [see Fig. 1(a) and (b)]. The two ends of the microstrip line [see Fig. 1(a)] extend into two broadband CPW-microstrip line transitions [see Fig. 1(c)]. The arrangement permits accurate measurement of the S-parameters of the device through CPW probes on a probe-station (Fig. 2) as a bias voltage is applied via one of the probes connected to an appropriate broadband bias tee.

This article has been accepted for inclusion in a future issue of this journal. Content is final as presented, with the exception of pagination.

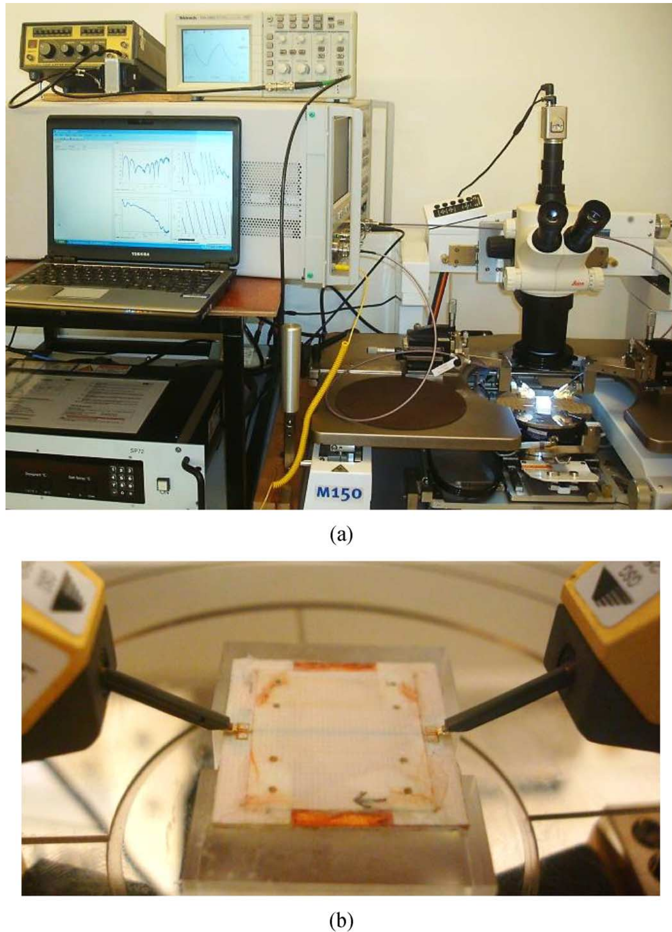

(a)

(b)

Fig. 2. Photographs of the: (a) complete measurement setup and (b) filled LC test device on the probe station chuck.

The dielectric layers in the two-layer LC test device (Fig. 1) have $h = 101$ μm and $\varepsilon_r = 3.66$. The LC layer formed between the two transitions has a length of $L = 7000$ μm. The dimensions of the patterned conductor in each transition are $W_T = 600$ μm, $W = 185$ μm, $G_1 = 700$ μm, $G_2 = 800$ μm, $S = 80$ μm, $d = 400$ μm, $L_1 = 1607$ μm, and $L_T = 2500$ μm. L_T is approximately equal to λ_g (guide wavelength) in the dielectric layers at 65 GHz and around $\lambda_g/4$ at 15 GHz. The CPW terminals are designed to be 50 Ω, matching the impedance of the CPW probes on the probe stations. The width (W_T) and the thickness (h) of the LC section (cell) is selected to meet condition $W_T \gg h$. This condition warrants that the electric field at the strip edges contributes little to the capacitance between the strip and the ground plane. This effect is an advantage in this case because at the bias voltages of 0 V and the fully switch-on voltage, V_{FS}, of the LC, the measured effective dielectric constants of the LC cell approximately represent the values of $\varepsilon_{r\perp}$ and $\varepsilon_{r||}$, as explained later. Increasing ε_r and h of the top substrate increases the effect of the field at the electrode edges, widening the difference between the measured effective permittivities and the values of $\varepsilon_{r\perp}$ and $\varepsilon_{r||}$. However, more accurate values can be extracted using a finite-element computer program developed by the authors [25].

Standard photolithography is used to fabricate the test device. The top dielectric layer (superstrate) on which the strip is etched and the supporting dielectric layer on which the transition conductors are patterned are Rogers 4350B substrate (Rogers Corporation, Rogers, CT, USA). As mentioned in Section I, the preconditioning of the faces of the LC cell is necessary. To this end, the superstrate on its strip face and the ground plane facing the LC are spin-coated with a thin passivation layer of polyimide to make these surfaces plane and smooth to submicrometer level. With the aid of a rubbing machine, the polyimide-covered surfaces, touching the LC under test, are rubbed longitudinally (along the microstrip line) and in an antiparallel manner [23]. This rubbing process generates lined groves of depths of a few nanometers. This standard preconditioning of the surfaces provides the LC molecules in the test device with correct alignment and anchoring along the groves in the absence of the bias voltage (0 V). At a sufficiently high bias voltage (V_{FS}) the directors under the microstrip line, preconditioned parallel to the longitudinal direction, effectively turn into perpendicular direction to the strip. For the prototype devices, silver epoxy paste is used to make contact between the main ground plane and the CPW grounds [see Fig. 1(d)] and to connect the microstrip in the LC cell to the transition middle strip. It was found by the simulation and measurement that the silver epoxy paste protruding out by an extra 20 μm from the CPW ground connection level had little effect on the measurements. With careful fabrication the bulging of the paste is much less and is around a few micrometers. As regards the connection between the transition center strip and microstrip line, a semi-circle is patterned at the end of each line so that when the ends of the two lines touch each other an empty circle is formed [see Fig. 1(c)]. This circle is carefully filled with epoxy. To experiment the possibility of spillage of silver epoxy to the surrounding area, a glass plate was used as the superstrate in a test cell and we observed that with some care in the fabrication no silver epoxy leaked out of the circle. With the aid of registration holes, the prepared dielectric layers and the ground plane are assembled. The device is filled with the LC under test using a fine syringe through the gap on the side of the device shown in Fig. 1(b). The large air-escape gap in the opposite side of the device [see Fig. 1(a)] disperses and eliminates any possible air bubbles during the filling process. Furthermore, any bubbles near or under the electrodes (strip and ground plane) can be readily detected by the time-domain reflectometry (TDR) technique available on many modern vector network analyzers (VNAs). We have tried this and no bubbles have been detected. The procedure has also been found to give bubble-free filling on a test cell with a glass plate instead of the ground plane, used to verify the alignment and the production of bubbles.

III. S-Parameters of Transitions

Having the S-parameters of the LC cell leads to determination of the electrical properties of the LC under test. However, the measurement of S-parameters of the test device involves those of the two identical CPW to microstrip line transitions and the cell (Fig. 1). To de-embed the contributions of the transitions from the measurement of the device, their S-parameters need to be determined. For this purpose, after appropriate modifications, the two-tier thru-line (TL) technique introduced in [26]

This article has been accepted for inclusion in a future issue of this journal. Content is final as presented, with the exception of pagination.

and [27] is applied. In this technique, the thru and line standards are needed. These symmetrical standards have transitions exactly the same as those in the test device. The thru standard is realized by arranging the transitions back to back and the line standard by patterning a length (l) of the microstrip line between the two back-to-back transitions.

The transmission matrices $[T]_{\mathrm{thru}}$ and $[T]_{\mathrm{line}}$ of the thru and the line can therefore be stated as

$$[T]_{\mathrm{thru}} = [T]_{\mathrm{trans}}[T]_{\mathrm{revtrans}} \tag{2a}$$

$$[T]_{\mathrm{line}} = [T]_{\mathrm{trans}}[T]_{\mathrm{delay}}[T]_{\mathrm{revtrans}} \tag{2b}$$

where $[T]_{\mathrm{trans}}$ and its reverse $[T]_{\mathrm{revtrans}}$ denote the transmission matrices for the two identical transitions as in Fig. 1(c) in forward and reverse order, and $[T]_{\mathrm{delay}}$ is the transmission matrix for the length (l) of the microstrip line. These matrices are given by

$$[T]_{\mathrm{trans}} = \frac{1}{S_{21}}\begin{bmatrix} 1 & -\mathrm{S}_{22} \\ \mathrm{S}_{11} & \mathrm{S}_{21}^2 - \mathrm{S}_{11}\mathrm{S}_{22} \end{bmatrix} \tag{3a}$$

$$[T]_{\mathrm{revtrans}} = \frac{1}{S_{21}}\begin{bmatrix} 1 & -\mathrm{S}_{11} \\ \mathrm{S}_{22} & \mathrm{S}_{21}^2 - \mathrm{S}_{11}\mathrm{S}_{22} \end{bmatrix} \tag{3b}$$

$$[T]_{\mathrm{delay}} = \begin{bmatrix} \mathrm{e}^{\gamma l} & 0 \\ 0 & \mathrm{e}^{-\gamma l} \end{bmatrix} \tag{3c}$$

where S_{11}, S_{22}, and S_{21} denote the S-parameters of the transitions and $\gamma = \alpha + j\beta$ is the complex propagation constant of the wave in the delay section. Of course (3) is correct as long as the losses are assumed small, the transitions identical, and the standards reciprocal.

The thru and line transmission matrices in (2) can be expressed in terms of the S-parameters of the two symmetrical standards (ρ and τ for the thru and ρ' and τ' for the line standard) as follows:

$$[T]_{\mathrm{thru}} = \frac{1}{\tau}\begin{bmatrix} 1 & -\rho \\ \rho & \tau^2 - \rho^2 \end{bmatrix} \tag{4a}$$

$$[T]_{\mathrm{line}} = \frac{1}{\tau}\begin{bmatrix} 1 & -\rho' \\ \rho' & \tau'^2 - \rho'^2 \end{bmatrix}. \tag{4b}$$

The thru and line standards are assumed to have port impedances matched to the VNA ports, and hence, ρ and ρ' as well as τ and τ' are the reflection and transmission coefficients measured. Using (2)–(4), S_{11}, S_{22}, and S_{21} of the transitions can be determined [26], [27],

$$S_{11} = \frac{\tau\rho' - \tau'\rho e^{-\gamma l}}{\tau - \tau' e^{-\gamma l}} \tag{5a}$$

$$S_{22} = \frac{\rho - \rho'}{\tau - \tau' e^{-\gamma l}} \tag{5b}$$

$$S_{21}^2 = \frac{\tau\tau'(e^{\gamma l} - e^{-\gamma l})}{\tau - \tau' e^{-\gamma l}}. \tag{5c}$$

As defined earlier, $\gamma = \alpha + j\beta$ is found by using (3) in (2),

$$\alpha = \left| \mathrm{Re}\left[\frac{1}{l}\ln\left(\frac{D - 2 \pm \sqrt{D^2 - 4D}}{2}\right)\right]\right| \tag{6a}$$

$$\beta = \left| \mathrm{Im}\left[\frac{1}{l}\ln\left(\frac{D - 2 \pm \sqrt{D^2 - 4D}}{2}\right)\right]\right| \tag{6b}$$

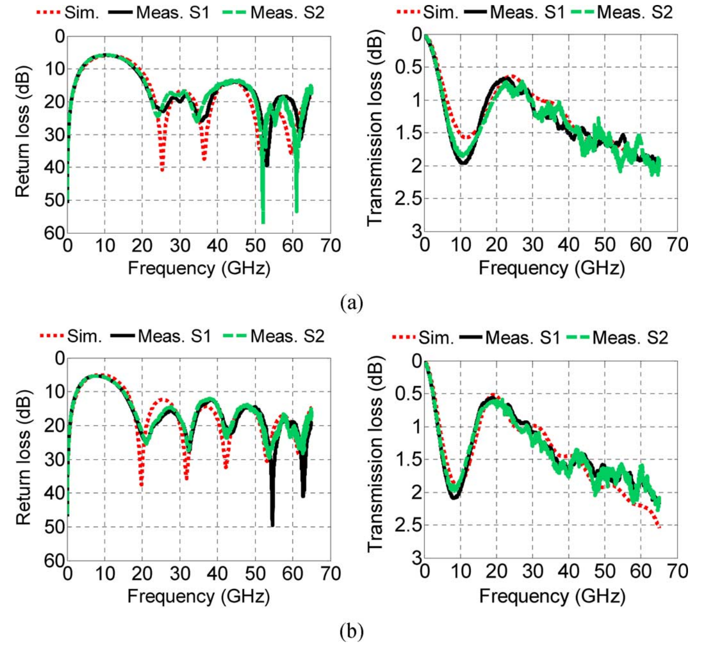

Fig. 3. Measured and simulated transmission and return losses of the: (a) thru and (b) line (1-mm line) standards for two fabricated sets.

where $D = \det\left([T]_{\mathrm{thru}} + [T]_{\mathrm{line}}\right)$.

Using the aforementioned two-tier de-embedding technique, the scattering parameters of the identical transitions in the test device (Fig. 1) specified in Section II were obtained. To this end, first the thru and line standards having transitions with the same physical and electrical specifications as those in the LC test device were fabricated. For the line standard, the delay length selected is $l = 1$ mm. The measurement system is shown in Fig. 2.

Fig. 3 shows the transmission and reflection coefficients (S-parameters in this case) over a wide range of frequencies for two fabricated sets S1 and S2 of the thru and line standards, obtained by measurements and by CST Microwave Studio Suite 2014 software (CST GmbH, Darmstadt, Germany). The reason for the two sets is to test the repeatability of the design and fabrication. Generally, the simulations and experiments appear to be in good agreement. Some discrepancies observed between the measurement and simulation results are attributable to the production process and shortcomings of the simulation software.

Equation (5) is then applied to both measured and simulated results shown in Fig. 3 of the thru and line standards. In the process, all the necessary equations were implemented in MATLAB (Mathworks, Natick, MA, USA) taking care of magnitude and phase values. The extracted S-parameters of the single transition obtained from the two sets of measurements and simulation data are shown in Fig. 4. Although they are generally in good agreement, it was observed that measured $|S_{21}|$ had less good agreement for frequencies smaller than 15 GHz. After careful examination of the technique, this is attributed to the measurement error. In fact, at low frequencies, the behavior of the thru standard (with zero delay line) and line standard (with $l = 1$ mm delay line) are similar as seen in Fig. 3, and hence, slight VNA errors in the measurement of their

This article has been accepted for inclusion in a future issue of this journal. Content is final as presented, with the exception of pagination.

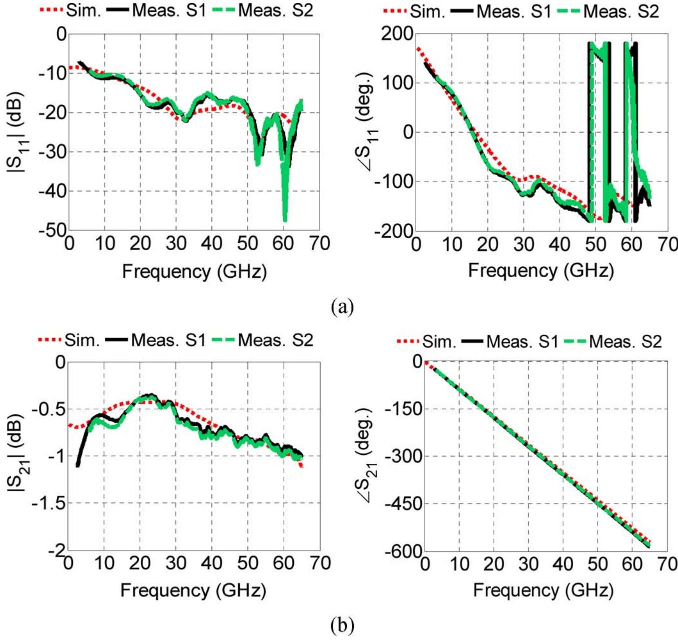

Fig. 4. S-parameters of the transition extracted from measurements and simulations (Fig. 3) for two fabricated sets: (a) S_{11} magnitude and phase and (b) S_{21} magnitude and phase.

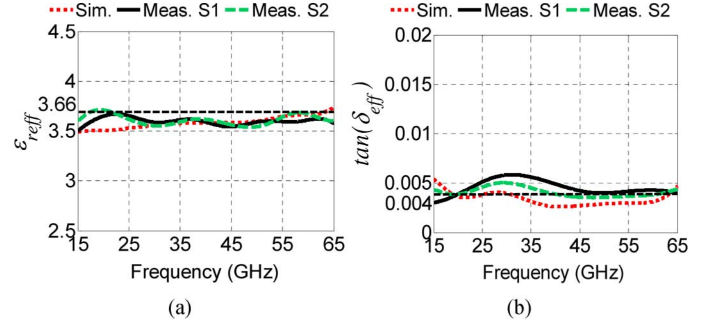

Fig. 5. Measured and simulated: (a) ε_{reff} and (b) $\tan(\delta_{\text{eff}})$ of the delay section for two fabricated sets of the (1-mm long) line standard.

S-parameters would affect the accuracy of the S-parameters extracted for the transition at low frequencies.

To further verify the accuracy of the two-tier de-embedding technique in practice, the effective dielectric constant, $\varepsilon_{reff} = (\beta\lambda_0/2\pi)^2$, and the effective loss tangent, $\tan(\delta_{\text{eff}}) = (\alpha - \alpha_C)(\lambda_0/\pi\sqrt{\varepsilon_{reff}})$ [28], of the delay section were also computed using (6) in conjunction with the measurement data for the two sets of the thru and line in Fig. 3 and they are shown in Fig. 5 along with those from the simulation. In the preceding expressions, λ_0 is the free-space wavelength and $\alpha_C = (R_s\sqrt{\varepsilon_{reff}}/\eta_0 h)$ is the attenuation due to the electrodes in which the surface resistivity $R_s = \sqrt{\pi f\,\mu_0/\sigma\kappa}$. Since the electrodes (ground plane and the strip conductor) are copper, $\sigma = 5.7 \times 10^7$ S/m. For the surface roughness coefficient, κ, the assumption $\kappa = 1/K_{SR}^2$ is used where accurate expression for K_{SR} is developed and reported in [29] and [30]. In this work, the root mean square (rms) height of the rough surface profile of the copper on Rogers 4350B substrate is assumed $h_{rms} \approx 0.4$ μm as also verified by an atomic force microscope (AFM), following [22]. This value is considered in the expression for K_{SR}. As can be deduced from Fig. 5(a), if a maximum error of ±2.5% is acceptable (which is of the order of the calibration error of VNAs), ε_{reff} averages at 3.6 over frequencies above 15 GHz for the experimental results. This obtained value is very close to the true value of the dielectric constant (3.66) of the Rogers substrate used in the structure including in the delay section. The close agreement is due to $W_T \gg h$ specified for the delay section, rendering $\varepsilon_{reff} \rightarrow \varepsilon_r$ as the fringing field is small. Below 15 GHz, the error of the experimental results is higher than ±2.5%. Therefore, for practical purposes, the low-frequency limit of the transition is set at 15 GHz. Considering $\tan(\delta_{\text{eff}})$ in Fig. 5(b), both the simulation and measurement agree within the wide band of 15–65 GHz and are close to $\tan(\delta) = 0.004$ quoted for the Rogers substrate. The high-frequency limit of the transition is set by the effects of losses as (2)–(6) are derived for a low-loss structure considering a complex γ with a small real part. For the considered transition, it is set at 65 GHz as the theoretical and experimental results in Fig. 5 are in good agreement with the values in the data sheet of the Roger substrate, at least, to 65 GHz. The frequency limits specified for the transition is approximately valid for the test device (Fig. 1) too, as the transitions in the device are the main contributors to the losses (especially to radiation losses) at high frequencies and to measurement errors at low frequencies, as explained earlier.

IV. Extracting Dielectric Properties of LC

A. Extraction Technique

Considering that the LC test device comprises the LC cell, two transitions and two discontinuities between the transitions and the LC cell, its overall transmission matrix can be expressed by the following chain transmission matrix [22]:

$$[T] = [T]_{\text{trans}}[T]_{\text{dis}}[T]_{\text{LC}}[T]_{\text{revdis}}[T]_{\text{revtrans}}. \tag{7}$$

In (7), $[T]$ is determined from the measurement of the S-parameters of the device at each bias voltage, $[T]_{\text{trans}}$ and $[T]_{\text{revtrans}}$ are known (as they are extracted by the TL technique; Section III), and the transmission matrix for the LC cell is similar to that in (3),

$$[T]_{\text{LC}} = \begin{bmatrix} e^{\gamma_{\text{eff}}L} & 0 \\ 0 & e^{-\gamma_{\text{eff}}L} \end{bmatrix} \tag{8}$$

where $\gamma_{\text{eff}} = \alpha_{\text{eff}} + j\beta_{\text{eff}}$ is defined as the effective complex propagation constant of the wave in the filled LC cell. The transmission matrix $[T]_{\text{dis}}$ and its reverse form $[T]_{\text{revdis}}$ represent the discontinuities on the two ends of the LC cell and their approximate expressions can be found using [28]

$$[\text{T}]_{\text{dis}} = \frac{1}{2\sqrt{\beta\beta_{\text{eff}}}}\begin{bmatrix} \beta + \beta_{\text{eff}} & \beta - \beta_{\text{eff}} \\ \beta - \beta_{\text{eff}} & \beta - \beta_{\text{eff}} \end{bmatrix} \tag{9a}$$

$$[\text{T}]_{\text{revdis}} = \frac{1}{2\sqrt{\beta\beta_{\text{eff}}}}\begin{bmatrix} \beta + \beta_{\text{eff}} & -(\beta - \beta_{\text{eff}}) \\ -(\beta - \beta_{\text{eff}}) & \beta - \beta_{\text{eff}} \end{bmatrix} \tag{9b}$$

This article has been accepted for inclusion in a future issue of this journal. Content is final as presented, with the exception of pagination.

where β is defined by (6). In (9), β_{eff} corresponding to $\varepsilon_{r\text{LCeff}}$ represents the wave phase constant in the LC layer. It is important to note that the effective dielectric constant, $\varepsilon_{r\text{LCeff}}$, of the LC section varies as the cell is biased between 0 V and V_{FS} and it meets the condition $\varepsilon_{r\perp} < \varepsilon_{r\text{LCeff}} < \varepsilon_{r||}$ because the effects of fringing fields in this device is negligible.

For the two limiting cases of interest, the unswitched LC (bias voltage $V = 0$ V) and fully switched LC ($V = V_{\text{FS}}$), $\beta_{\text{eff}} \approx \beta_{\perp}$ and $\beta_{\text{eff}} \approx \beta_{||}$, respectively (considering preconditioned alignment of LC parallel to the wave propagation). For these cases, (9) is accurate ignoring small energy storage near the discontinuities; which indeed is negligible as the dielectric constant of the substrate of the transitions is close to the typical dielectric constant of nematic LCs.

After the de-embedding of the transitions, (7) leads to

$$[T]_{\text{trans}}^{-1}\,[T]\;[T]_{\text{revtrans}}^{-1} = [T]_{\text{dis}}[T]_{\text{LC}}[T]_{\text{revdis}}. \quad (10)$$

Considering low-loss LC materials, a program in MATLAB has been developed to solve (10) numerically using an iterative method (Newton–Raphson available in MATLAB) at each bias voltage to obtain the corresponding β_{eff} and α_{eff}. Hence, the effective dielectric constant [28] of the LC is

$$\varepsilon_{r\text{LCeff}} = \left(\frac{\beta_{\text{eff}}\lambda_0}{2\pi}\right)^2. \quad (11)$$

The attenuation constant, α_{eff}, includes the effect of LC losses, top layer dielectric losses, conductor losses, and any radiation losses from the LC cell. To isolate the losses arising from the LC alone, the LC test device was first measured with an empty LC cavity (filled with air, $\varepsilon_r = 1$). The $\alpha_{\text{aireff}} - \alpha_{\text{Cair}}$ (indicating the attenuation due to radiation and superstrate) of the air-filled cell where α_{Cair} is the attenuation due to the conductor losses in the empty LC cavity, is then subtracted from $\alpha_{\text{eff}} - \alpha_{C\text{LCeff}}$ (denoting the attenuation due to LC, radiation, and superstrate), where $\alpha_{C\text{LCeff}}$ is the conductor losses in the LC-filled cavity, to find (with a good approximation) the effective attenuation due to LC,

$$\alpha_{\text{LCeff}} = \alpha_{\text{eff}} + \alpha_{\text{Cair}}(1 - \sqrt{\varepsilon_{r\text{LCeff}}}) - \alpha_{\text{aireff}}. \quad (12)$$

To derive (12), the attenuation due to conductor losses of the microstrip line in the LC section (cell) is assumed to be given by $\alpha_C = (R_s\sqrt{\varepsilon_{\text{reff}}}/\eta_0 h)$; as indicated in the last paragraph of Section III. For the air-filled case, $\varepsilon_{\text{reff}} \approx 1$, and for the LC-filled case, $\varepsilon_{\text{reff}} = \varepsilon_{r\text{LCeff}}$. Expression (12) would provide a more accurate assessment of the dielectric losses of the LC under test as compared with [22]. In view of (12), $\tan(\delta_{\text{LCeff}})$ of the LC at different bias voltages can be obtained using [28],

$$\tan(\delta_{\text{LCeff}}) = \frac{2\alpha_{\text{LCeff}}\beta_{\text{eff}}}{\beta_{\text{eff}}^2 - \alpha_{\text{LCeff}}^2}. \quad (13)$$

B. Verification of Extraction Technique

Fig. 6(a) shows the effective dielectric constant ($\varepsilon_{\text{aireff}}$) obtained from (11) when the LC test device was measured air filled. The extracted dielectric constant is close to 1 with the maximum variation of 0.07 [see Fig. 6(a)]. Since the LC cell was air filled, the expected extracted permittivity value was 1, and hence, the value in Fig. 6(a) confirms the accuracy of the presented method. However, for the whole bandwidth of the device (15–65 GHz), the extracted permittivity generally stays slightly above 1 (maximum of 7%). The reason for this is the presence of the thin polyimide film on both the microstrip and ground conductors, which increases the overall permittivity. Fig. 6(b) shows the attenuation constant due to conductors for the air-filled LC cell. As expected, this attenuation increases with the frequency.

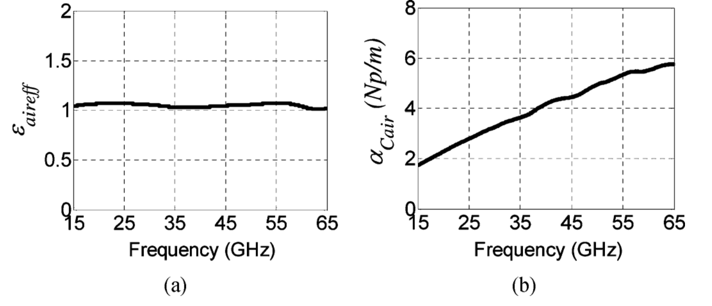

Fig. 6. (a) Dielectric constant and (b) attenuation constant due to conductors of the air-filled LC cell.

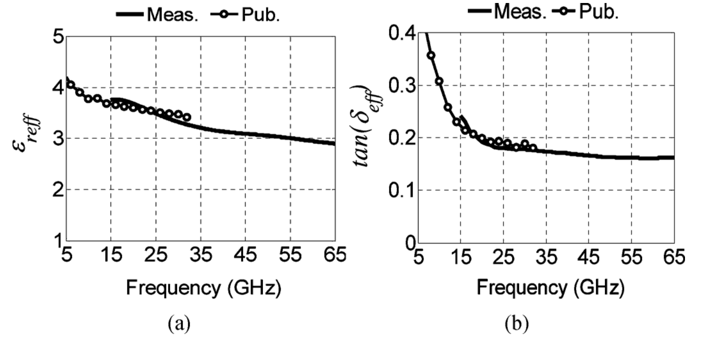

Fig. 7. (a) Dielectric constant and (b) loss tangent of LC cell containing Isopropanol; Pub. data from [31] and Meas. data from this work.

To demonstrate a further evidence that the analysis assumptions are correct, the dielectric constant and the loss tangent of Isopropanol were measured using the test device. The reason for the choice is the existence of reliable electrical data on this material [31]. In [31], the complex permittivity of Isopropanol over the frequency range of 1–32 GHz is reported. The dielectric constant and the loss tangent of Isopropanol extracted using the new test device together with those obtained from [31, Fig. 2] are shown in Fig. 7 over the frequency range of 5–65 GHz. As seen in the figure, the two sets of results are in very good agreement over the common measurement bandwidth of 15–32 GHz, and in fact, the maximum deviation between the corresponding results for the dielectric constant is 4.3% and for the loss tangent is 6.8%, as compared to the data from [31]. Considering Fig. 7, an extrapolation based on the set of results from [31] to frequencies beyond 32 GHz would predict that the dielectric constant and loss tangent of Isopropanol would vary slightly with frequency, and indeed this is in accord with the measured values from the present work.

This article has been accepted for inclusion in a future issue of this journal. Content is final as presented, with the exception of pagination.

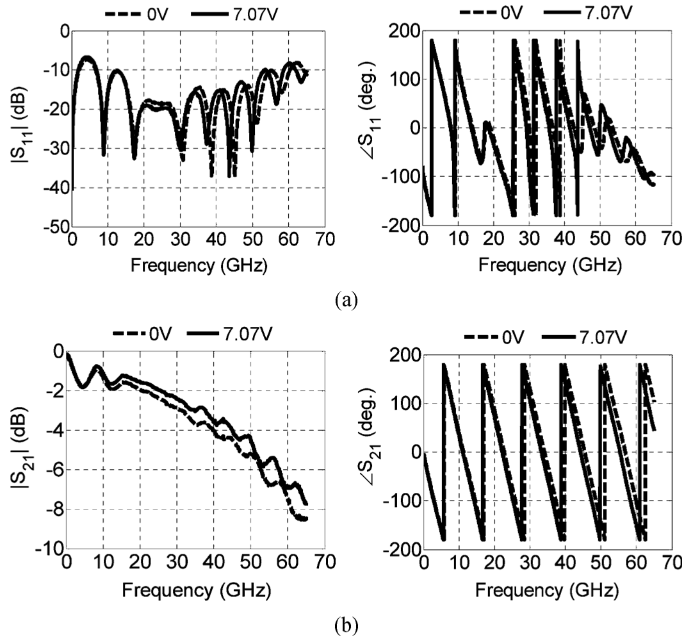

Fig. 8. Measured S-parameters of test device containing MDA-00-3506 at two bias voltages (in rms): (a) S_{11} mag. and phase and (b) S_{21} mag. and phase.

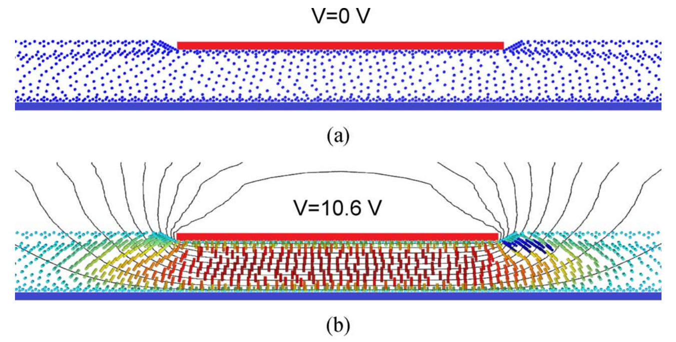

Fig. 9. Computer modeling of director orientation in the cross section of LC cell [see Fig. 1(a)] for GT3-23001 at: (a) 0 V (unswitched state) and (b) 10.6 V (switched state) for the longitudinal alignment. Dots (·) show director ends and bars (–) show turned directors. Color of the director indicates the tilt while the potential distribution is shown with contour lines.

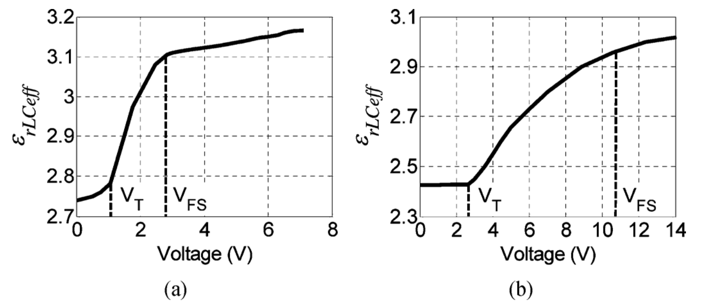

Fig. 10. Effective relative permittivities of LC cell versus bias voltage (in rms) at 65 GHz for: (a) MDA-00-3506 and (b) GT3-23001.

C. Extraction of Electrical Parameters of Two LCs

Next, the test device (having approximately 50-Ω CPW terminations over the bandwidth) was used to determine the dielectric properties of two different LCs, namely, MDA-00-3506 and GT3-23001. The latter has been specifically developed for RF applications [4]. The filled LC cell in the test device was biased using a low-frequency ac voltage (70 Hz) through a wideband bias tee inserted in line with one of the CPW probes in the probe station. In LCs, both dc and ac can be used for the bias voltage, but the ac voltage ensures that the ions are not formed in the LC [19]. The bias voltage was changed through 0–10 V in amplitude (0–7.07 Vrms) for MDA-00-3506 and through 0–20 V (0–14.14 Vrms) for GT3-23001. The latter LC requires higher voltage ($V_{\rm FS}$) to fully switch directors. The S-parameters of the test devices filled with the two LCs were measured for each bias voltage selected. As an example, the measured scattering parameters of the test device filled with MDA-00-3506 are shown in Fig. 8. In particular, Fig. 8(b) shows that the insertion loss reduces by stepping up the bias voltage from 0 to 7.07 V, implying that the dielectric losses associated with $\varepsilon_{||}$ should be smaller, i.e., $\tan(\delta_{||}) < \tan(\delta_{\perp})$. It should be noted that the change of the voltage changes the director direction from the default state (being in the direction parallel to electrodes along the wave propagation) to a nonuniform distribution largely perpendicular to the electrodes. A computer modeling [25] developed by the authors clearly shows this behavior for GT3-23001 (Fig. 9). The transmission phase on the other hand [see Fig. 8(b)] shows that the phase (delay) increases with the bias voltage, meaning $\varepsilon_{||} > \varepsilon_{\perp}$. These effects are generally expected with certain nematic LC materials [1]–[4].

Using (10)–(13), $\varepsilon_{r\rm LCeff}$, and $\tan(\delta_{\rm LCeff})$ of the MDA-00-3506 and GT3-23001 were extracted from the measured S-parameters (e.g., Fig. 8) of their test devices and are shown in Figs. 10–12. In Fig. 10, the switching and the change of $\varepsilon_{r\rm LCeff}$ with the bias voltage at a particular frequency (65 GHz) is clearly seen for the two LCs. The measured $\varepsilon_{r\rm LCeff}$ includes the effects of the bias voltage and the top substrate (superstrate) on the local dielectric property [or equivalently, the local director (Fig. 9)]. However, the effect of the superstrate is little, as $W_T \gg h$ is selected (causing electric field lines to accommodate highly between the strip width and the ground plane). As Fig. 10 shows, the LC cell has a threshold voltage, V_T, above which the reorientation of the LC molecules takes place. V_T relies on the ratio of elastic constant, K_{11}, to $\Delta\varepsilon_r$. For MDA-00-3506, Fig. 10(a), $V_T \approx 1$ V and above that there is a sharp rise in $\varepsilon_{r\rm LCeff}$ until the fully switch-on bias voltage of $V_{\rm FS} \approx 2.8$ V is reached. Above 2.8 V, the LC is almost fully reoriented and thus it exhibits little increase in $\varepsilon_{r\rm LCeff}$ (∼3%). The threshold voltage for GT3-23001 [see Fig. 10(b)] is considerably higher and is $V_T \approx 2.4$ V. The LC reaches its fully switch-on point at $V_{\rm FS} \approx 10.6$ V [see Fig. 10(b)]. Above this voltage, a further increase in $\varepsilon_{r\rm LCeff}$ is marginal (∼3%). Considering the mixed dielectric structure of the device (Fig. 1) and the nonuniform director distribution when the bias voltage is applied (Fig. 9), it is not difficult to understand that the actual $\varepsilon_{r||}$ of the LC under test will necessarily be slightly higher than $\varepsilon_{r\rm LCeff}$ obtained at the fully switch-on (or higher) voltages while the actual $\varepsilon_{r\perp}$ of the LC would be quite close to $\varepsilon_{r\rm LCeff}$ measured at 0 V since in that case the LC is uniformly aligned along the guide axis. For MDA-00-3506, this can be verified

This article has been accepted for inclusion in a future issue of this journal. Content is final as presented, with the exception of pagination.

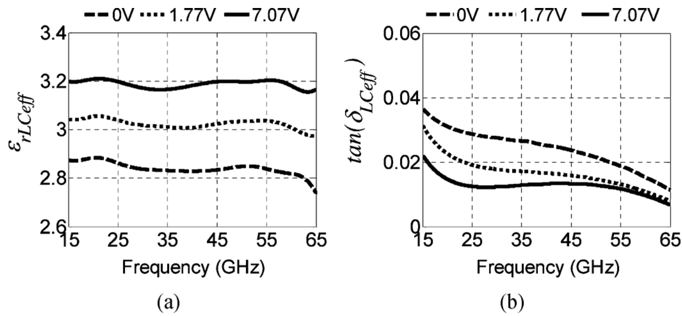

Fig. 11. Effective: (a) dielectric constants and (b) loss tangents of LC cell containing MDA-00-3506 versus frequency at three bias voltages (in rms).

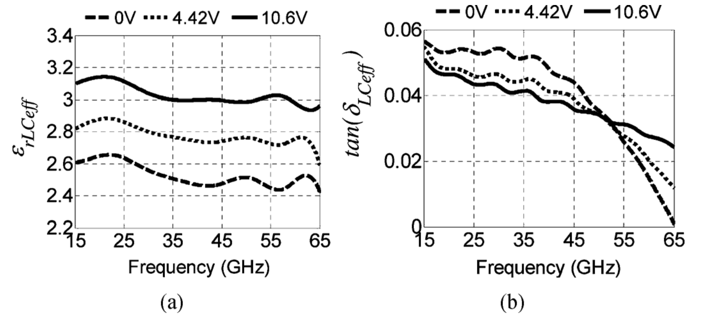

Fig. 12. Effective: (a) dielectric constants and (b) loss tangents of LC cell containing GT3-23001 versus frequency at three bias voltages (in rms).

by comparing the results in Fig. 10(a) with values of $\varepsilon_{r\perp}$ and $\varepsilon_{r||}$ in [22, Table III] given for 60 GHz.

For clarity, Figs. 11 and 12 are plotted for three different bias voltages over the frequency limits of the test device, 15–65 GHz. At 0-V bias, the LC cell is at the switch-off (default) state, and hence, $\varepsilon_{r\mathrm{LCeff}}$ and $\tan(\delta_{\mathrm{LCeff}})$ of the cell approximately equals $\varepsilon_{r\perp}$ and $\tan(\delta_{\perp})$ of the LC, while at rms voltages 7.07 V (for MDA-00-3506) and 10.6 V (for GT3-23001), the LC cells are in an acceptable switched state and $\varepsilon_{r\mathrm{LCeff}}$ and $\tan(\delta_{\mathrm{LCeff}})$ of the cell are approximately $\varepsilon_{r||}$ and $\tan(\delta_{||})$ of the LC.

When $\varepsilon_{r\perp}$ and $\varepsilon_{r||}$ inferred from Fig. 11(a) for MDA-00-3506 are compared with their accurate values in [22, Table III] at 60 GHz, the errors in the present approximate evaluations appears not to be more than 5% for $\varepsilon_{r||}$ and 1% for $\varepsilon_{r\perp}$, well within measurement uncertainties, as explained in Section V. Considering Fig. 11(b), $\tan(\delta_{\mathrm{LCeff}})$ follows the expected trend and decreases with frequency and bias voltage. When these results are compared with those in [22], the extracted $\tan(\delta_{\mathrm{LCeff}})$ in the present case has lower values by as much as a factor of 2.2. This is attributed to the effect of conductor and radiation losses eliminated from the final calculations in the present case (as explained earlier), and therefore, $\tan(\delta_{\mathrm{LCeff}})$ for the default and switch-on states provides closer estimates to the actual $\tan(\delta_{\perp})$ and $\tan(\delta_{||})$ of the LC. It should be noted that the present test device and method characterize the nematic LCs within a bandwidth of 15–65 GHz as compared to 30–60 GHz reported in [22], and therefore, provide an additional 20 GHz of LC characterization data, eliminating the need for different test devices with different bandwidths.

Fig. 12 shows the extracted effective dielectric constants and dielectric losses for GT3-23001. This LC is relatively new, and therefore, this is the first time that such a broadband characterization is conducted on GT3-23001. However, some specific characterizations of GT3-23001 using resonator, frequency-selective-surface, and coaxial-line techniques are covered in [12], [32], and [33]. Especially, based on the resonator technique, reported in [12] are values of $\varepsilon_{\perp}$, $\tan(\delta_{\perp})$, $\varepsilon_{||}$, and $\tan(\delta_{||})$ of GT3-23001 at 19 GHz and 1 kHz. Comparing $\varepsilon_{\perp}$ and $\varepsilon_{||}$ from [12] with the present $\varepsilon_{r\mathrm{LCeff}}$ measured at the default (0 V) and switch-on (10.6 V) states at 19 GHz, Fig. 12(a), respectively, it is revealed that the maximum difference between the two sets of data is 0.15 (corresponding to an average error of 5.3%). As mentioned earlier, the measured effective dielectric constants at the two limiting voltages are close approximations to the actual $\varepsilon_{\perp}$ and $\varepsilon_{||}$. However, for this case, the optimization technique introduced in [25] was applied to the extracted effective dielectric constants to improve the accuracy. The improved values were found to be within the 4% of those reported by the resonance technique at 19 GHz [12].

Examining the dielectric losses of GT3-23001 [see Fig. 12(b)], some interesting results can be seen. As expected, the losses of this LC decrease with frequency. However, beyond 51 GHz, while the LC losses fall with the frequency, the losses at high bias voltage associated with $\varepsilon_{||}$ is higher than the loss at the low bias voltage associated with $\varepsilon_{\perp}$. Since normally $\tan(\delta_{\perp}) > \tan(\delta_{||})$ for nematic LCs, this anomaly may be either due to the relaxation effects in the LC [1] or to the chemical formulation of GT3-23001. The present extracted loss tangents of GT3-23001 differs from those reported in [12] at 19 GHz by a factor of 3.8 for $\tan(\delta_{\perp})$ and 10 for $\tan(\delta_{||})$. For this reason and as a further check, the dielectric losses of GT3-23001 were re-evaluated using a different LC test device reported in [22] by which several LCs characterized previously accurately. This trial revealed that the results extracted by the present device and that in [22] were of good match and the measured losses by the device in [22] showed a similar anomaly as seen in Fig. 12(b).

V. Uncertainty Analysis

The main errors originate from fabrication limitations and measurement system. Considering the fabrication of the (identical) transitions (Sections II and III), the transfer of the conductor patterns of the transitions from the photo-mask to the substrate using contact photolithography is repeatable to better than 12-μm accuracy in width and length. As the smallest dimension of the copper width in the (identical) transitions is $W = 185$ μm in Fig. 1, a maximum error of 6.5% can occur in the conductor patterning. Since each transition involves a tapered section and the taper performance is generally insensitive to slight variations to its design, the error in the conductor patterning was found to have a small effect on the performance of the (identical) transitions fabricated. However, the main problem in the fabrication of the measurement standards including the transitions as well as the fabrication of the LC test device is in their assembly as there are four vias from the microstrip ground to CPW ground. These are formed using silver epoxy paste (Fig. 1). Simulation shows that the silver epoxy

This article has been accepted for inclusion in a future issue of this journal. Content is final as presented, with the exception of pagination.

paste protruding out of the connection holes must be less than 20 μm in height. By careful fabrication and with the right skill, the height can be easily controlled to less than 5 μm. Therefore, in practice, near identical transitions are achievable for the line and thru standards, as well as for the LC test device.

The measurement system errors are due to the calibration error of the VNA, which is better than 2.7% over 1–65-GHz bandwidth for the VNA used in this work, and due to the landing position error of the probes in the probe station. With our manual probing system, the maximum landing position error is 15 μm for an experienced operator, but with automated probe systems this error can be much smaller. The CPW terminal ends [see Fig. 1(a)] on the LC device and on the thru/line standards are used as the references to position the probes. As the highest measurement frequency is 65 GHz corresponding to $\lambda_g \approx 2500$ μm (as in Section II), the maximum landing position error translates to about 4° of phase uncertainty in the transmission phase ($\angle S_{21}$), which is the maximum phase uncertainty over the band of interest. Therefore, considering that the total transition length is $L_1 + L_T = 4107$ μm (Fig. 1), the worst phase error expected is less than 1% for a transition.

Fig. 3 shows the measurements of the S-parameters of two sets (S1 and S2) of the thru and line samples involving eight (ideally identical) transitions. In this experiment, the VNA was calibrated separately for each set of samples to exaggerate the variation of the calibration error. It is clear from Fig. 3 that the measurements have indeed very close agreement with a maximum inconsistency of about 11% under and 5% over the 15-GHz delineation. This trend is also true for those in Fig. 4 dedicated to the extracted S-parameters of the transition. When the VNA is calibrated once and both sets of samples are measured, the agreement is better than 4.5%.

The preceding errors involved in the characterization of the transition can be reflected in an overall error by considering that the errors in the fabrication and in the measurement system including the VNA calibration error and landing position error are ultimately manifested in an (upper bound) error in the extraction of the dielectric constant and loss tangent of the known dielectric substrate used in the structures of the thru and line standards. As discussed and shown by an example in Section III, this overall error due to uncertainties in the fabrication and measurement is about $\pm 2.5\%$ (5%).

As far as the measurement of the LC test device is concerned, in addition to the overall error, there would be some uncertainty owing to the locations of the two discontinuities at the ends of the LC cell in the device, Section II. This fabrication uncertainty is about 160 μm for the two discontinuities in the worst case. As the length of the LC cell is long ($L = 7000$ μm), the maximum error committed in the length, affecting (8), is small and less than 2.3%. One other uncertainty introduced by the fabrication of the test device is the quality of rubbing, which produces the nanometer groves in the polyimide treated device surfaces for anchoring and aligning the LC under test. However, with modern rubbing machines, this error is almost negligible.

Therefore, assuming a linear summation of the errors due to the fabrication and measurement, the maximum error in determining the dielectric constant and loss tangent of a nematic LC should not exceed 7.3% (5% + 2.3% from the preceding analyses). According to our experience, this is a safe, but overestimated error and normally the total error observed was around 5% for several LC measured, whose dielectric constants and loss tangents were known. Finally, the device and the measurement technique are robust, as together they have been successful in extracting the dielectric constants of several LC and non-LC materials within the measurement accuracy quantified in this section over a 15–65-GHz band.

VI. Conclusion

A new device for the broadband measurement of the dielectric constants and loss tangents of nematic LCs at microwave and millimeter-wave frequencies was proposed. This device, which has a simple microstrip structure, consists of two very thin dielectric layers to reduce radiation losses and has CPW terminals for easy measurement by a probe station. The connection between each terminal and the microstrip line is through a broadband transition. The specification of the device and its fabrication were outlined. Compared to previous test devices, the proposed device is extremely broadband with a practical bandwidth of 15–65 GHz. It has a solid exposed ground plane for easy temperature test and it operates under the bias voltage. A mathematical technique for de-embedding the effects of the transitions from the device was presented. The extraction process for obtaining the dielectric parameters of LCs by this device was then explained. Two different nematic LCs, MDA-00-3506 and GT3-23001, were characterized and their measured dielectric constants were found to be within 5% and 5.3% of those available in the literature. As shown in one example, the device can also be used for accurate characterization of normal low-loss liquids.

References

[1] J. K. P. J. Collings and M. Hird, *Introduction to Liquid Crystals: Chemistry and Physics*. London, U.K.: CRC, 1997.

[2] S. Wu and D. Yang, *Fundamentals of Liquid Crystal Devices*. West Sussex, U.K.: Wiley, 2006.

[3] P. G. De Gennes and J. Prost, *The Physics of Liquid Crystals*. Oxford, U.K.: Oxford Univ. Press, 1993.

[4] A. Manabe, "Liquid crystals for microwave applications," in *Proc. Eur. Conf. Antennas Propag. (EUCAP)*, Göteborg, Sweden, Apr. 2013, pp. 1734–1735.

[5] T. Kuki, H. Fujikake, and T. Nomoto, "Microwave variable delay line using dual-frequency switching-mode liquid crystal," *IEEE Trans. Microw. Theory Techn.*, vol. 50, no. 11, pp. 2604–2609, Nov. 2002.

[6] C. Fritzsch, F. Giacomozzi, O. H. Karabey, S. Bildik, S. Colpo, and R. Jakoby, "Advanced characterization of a W-band phase shifter based on liquid crystals and MEMS technology," *Int. J. Microw. Wireless Technol.*, vol. 4, pp. 379–386, Jun. 2012.

[7] N. Martin, P. Laurent, C. Person, P. Gelin, and F. Huret, "Patch antenna adjustable in frequency using liquid crystal," in *Proc. Eur. Microw. Conf. (EUMC)*, Munich, Germany, Oct. 2003, pp. 699–702.

[8] W. Hu, R. Cahill, J. A. Encinar, R. Dickie, H. Gamble, V. Fascco, and N. Grant, "Design and measurement of reconfigurable mm-wave reflect-array cells with nematic liquid crystal," *IEEE Trans. Antennas Propag.*, vol. 56, no. 10, pp. 3112–3117, Oct. 2008.

[9] E. Doumaines, R. Dickie, P. Baine, G. Perez-Palomino, R. Cahill, G. Goussetis, J. A. Encinar, M. Barba, S. Christie, N. Mitchell, M. Bain, and G. Toso, "Nematic liquid crystals for reconfigurable mm-wave antenna technology," in *Proc. Eur. Conf. Antennas Propag.*, Göteborg, Sweden, Apr. 2013, pp. 1791–1792.

This article has been accepted for inclusion in a future issue of this journal. Content is final as presented, with the exception of pagination.

[10] A. Gaebler, A. Moessinger, F. Goelden, A. Manabe, M. Goebel, R. Follmann, D. Koether, C. Modes, A. Kipka, M. Deckelmann, T. Rabe, B. Schulz, P. Kuchenbecker, A. Lapanik, S. Mueller, W. Haase, and R. Jakoby, "Liquid crystal reconfigurable antenna concepts for space applications at microwave and millimeter waves," *Int. J. Antennas Propag.*, vol. 2009, 2009, Article ID 876989.
[11] V. F. Fusco, R. Cahill, W. Hu, and S. Simms, "Ultra-thin tuneable microwave absorber using liquid crystals," *Electron. Lett.*, vol. 44, no. 1, pp. 37–38, Jan. 2008.
[12] P. Yaghmaee, C. Fumeaux, B. Bates, A. Manabe, O. H. Karabey, and R. Jakoby, "Frequency tunable S-band resonator using nematic liquid crystal," *Electron. Lett.*, vol. 48, no. 13, pp. 798–800, Jun. 2012.
[13] M. Yazdanpanahi and D. Mirshekar-Syahkal, "Millimeter-wave liquid-crystal-based tunable bandpass filter," in *Proc. IEEE Radio Wireless Symp.*, Santa Clara, CA, USA, Jan. 2012, pp. 139–142.
[14] F. Goelden, S. Mueller, P. Scheele, M. Wittek, and R. Jakoby, "IP3 measurements of liquid crystals at microwave frequency," in *Proc. Eur. Microw. Conf.*, Manchester, U.K., Oct. 2006, pp. 971–974.
[15] A. Giere, P. Scheele, Y. Zheng, and R. Jakoby, "Characterization of the field-dependent permittivity of nonlinear ferroelectric films using tunable coplanar lines," *IEEE Microw. Wireless Compon. Lett.*, vol. 17, no. 6, pp. 442–444, Jun. 2007.
[16] Y. Poplavko, Y. Prokopenko, V. Pashkov, V. Molchanov, I. Golubeva, V. Kazmirenko, and D. Smigin, "Low loss microwave piezo-tunable devices," in *Proc. Eur. Microw. Conf.*, Manchester, U.K., Oct. 2006, pp. 657–660.
[17] A. Penirschke, S. Muller, P. Scheele, C. Weil, M. Wittek, C. Hock, and R. Jakoby, "Cavity perturbation method for characterization of liquid crystals up to 35 GHz," in *Proc. Eur. Microw. Conf.*, Amsterdam, The Netherlands, Oct. 2004, pp. 545–548.
[18] Y. Utsumi and T. Kamei, "Dielectric permittivity of liquid crystal in the microwave and millimetre range," *Molecular Crystals and Liquid Crystals*, vol. 409, pp. 355–370, Jan. 2004.
[19] M. Yazdanpanahi, S. Bulja, D. Mirshekar-Syahkal, R. James, S. E. Day, and F. A. Fernandez, "Measurement of dielectric constants of nematic liquid crystals at mm-wave frequencies using patch resonator," *IEEE Trans. Instrum. Meas.*, vol. 59, no. 12, pp. 3079–3085, Dec. 2010.
[20] S. Mueller, A. Penirschke, C. Damm, P. Scheele, M. Wittek, C. Weil, and R. Jakoby, "Broad-band microwave characterization of liquid crystals using a temperature-controlled coaxial transmission line," *IEEE Trans. Microw. Theory Techn.*, vol. 53, no. 6, pp. 1937–1944, Jun. 2005.
[21] S. Mueller, M. Koerble, F. Goelden, A. Penirschke, A. Gaebler, A. Lapanik, and R. Jakoby, "W-band characterization of anisotropic liquid crystals at room temperature," in *Proc. Eur. Microw. Conf.*, Amsterdam, The Netherlands, Oct. 2008, pp. 119–122.
[22] S. Bulja, D. Mirshekar-Syahkal, R. James, S. Day, and F. A. Fernandez, "Measurement of dielectric properties of nematic liquid crystals at millimeter wavelength," *IEEE Trans. Microw. Theory Techn.*, vol. 58, no. 12, pp. 3493–3501, Dec. 2010.
[23] S. Ishihara, "How far has the molecular alignment of liquid crystals been elucidated," *J. Display Technol.*, vol. 1, no. 1, pp. 30–40, Sep. 2005.
[24] C. W. Oseen, "The theory of liquid crystals," *Trans. Faraday Soc.*, vol. 29, pp. 883–898, 1933.
[25] R. James, F. A. Fernández, S. E. Day, S. Bulja, and D. Mirshekar-Syahkal, "Accurate modeling for the wideband characterization of nematic liquid crystals for microwave applications," *IEEE Trans. Microw. Theory Techn.*, vol. 57, no. 12, pp. 3293–3297, Dec. 2009.
[26] A. Cosu, G. Gilardi, P. Tommasino, A. Trifiletti, and A. Vannucci, "A method for microwave characterization of LiNbO modulators," *IEEE Microw. Wireless Compon. Lett.*, vol. 13, no. 2, pp. 60–62, Feb. 2003.
[27] S. Bulja and D. Mirshekar-Syahkal, "Novel wide-band transition between coplanar waveguide and microstrip line," *IEEE Trans. Microw. Theory Techn.*, vol. 58, no. 7, pp. 1851–1857, Jul. 2010.
[28] R. E. Collin, *Foundations for Microwave Engineering*, 2nd ed. New York, NY, USA: McGraw-Hill, 2008.
[29] L. Tsang, H. Braunisch, R. Ding, and X. Gu, "Random rough surface effects on wave propagation in interconnects," *IEEE Trans. Adv. Packag.*, vol. 33, no. 4, pp. 839–856, Nov. 2010.
[30] D. E. Zelenchuk, V. Fusco, G. Goussetis, A. Mendez, and D. Linton, "Millimeter-wave printed circuit board characterization using substrate integrated waveguide resonators," *IEEE Trans. Microw. Theory Techn.*, vol. 60, no. 10, pp. 3300–3308, Oct. 2012.
[31] S. Seo, T. Stintzing, I. Block, D. Pavlidis, M. Rieke, and P. G. Layer, "High frequency wideband permittivity measurements of biological substrates using coplanar waveguides and application to cell suspensions," in *IEEE MTT-S Int. Microw. Symp. Dig.*, 2008, pp. 915–918.
[32] R. Dickie, P. Baine, R. Cahill, E. Doumanis, G. Goussetis, S. Christie, N. Mitchell, V. Fusco, D. Linton, J. Encinar, R. Dudley, D. Hindley, M. Naftaly, M. Arrebola, and G. Toso, "Electrical characterisation of liquid crystals at millimetre wavelengths using frequency selective surfaces," *Electron. Lett.*, vol. 48, no. 11, pp. 611–612, May 2012.
[33] W. Hu, O. H. Karabey, A. E. Prasetiadi, M. Jost, and R. Jakoby, "Temperature controlled artificial coaxial line for microwave characterization of liquid crystal," in *Proc. German Microw. Conf.*, Aachen, Germany, Mar. 2014, 4 pp.

Prafulla Deo (M'11) received the B.Eng. degree in electronics and communication from the University Institute of Technology, Barkatullah University, Bhopal, India, in 2002, the M.Sc. degree in telecommunication and information systems from the University of Essex, Colchester, U.K., in 2005, and the Ph.D. degree in advanced telecommunications from Swansea University, Swansea, U.K., in 2011.

From 2009 to 2014, he was a Senior Research Officer with the School of Computer Science and Electronic Engineering, University of Essex, where he was involved with the characterization and applications of liquid-crystal (LC) materials at microwave and millimeter-wave frequencies. Since 2014, he has been a Postdoctoral Research Associate with the Jodrell Bank Centre of Astrophysics, The University of Manchester, Manchester, U.K., where he is involved in the design and development of quasi-optical and RF components for space and astronomical applications. His current research interests include microwave and millimeter-wave antennas and devices, LC-based antennas, antenna arrays, phase shifters, and other associated components for microwave and millimeter-wave frequency bands, beam-steerable antennas, and high-impedance surfaces/electromagnetic-bandgap structures and their antenna applications.

Dariush Mirshekar-Syahkal (F'14) received the B.Sc. degree (with distinction) in electrical engineering from Tehran University, Tehran, Iran, in 1974, and the M.Sc. degree in microwaves and modern optics and Ph.D. degree from University College London, University of London, London, U.K., in 1975 and 1979, respectively.

From 1979 to 1984, he was a Reseach Fellow with University College London, where he was involved with the analysis and design of microwave and millimeter-wave planar transmission lines and components, as well as on nondestructive evaluation of materials by electromagnetic techniques. Since 1984, he has been a staff member with the University of Essex, Colchester, UK, where he is currently a Professor and the Head of the RF and Microwave Research Laboratory, School of Computer Science and Electronic Engineering. He has been a consultant to over ten major international companies. He has authored or coauthored numerous technical publications including *Spectral Domain Method for Microwave Integrated Circuits* (Wiley, 1990). He holds several patents. His current research includes super-compact filters for ultra-wideband (UWB) miniaturized systems, adaptive antennas, numerical modelings for electromagnetic (EM) problems, and characterization and applications of liquid-crystal materials at microwave and millimeter-wave frequencies in which research field he has led two joint projects.

Professor Mirshekar is a Chartered Engineer. He is a Fellow of the IET.

This article has been accepted for inclusion in a future issue of this journal. Content is final as presented, with the exception of pagination.

Lawrence Seddon received the B.Sc. (hons) degree in computer science from the University of Kent, Canterbury, U.K., in 1987, the B.Sc. (hons) degree in mathematical physics from the University of Edinburgh, Edinburgh, U.K., in 2004, the M.Sc. degree in applied mathematical sciences from Heriot-Watt University, Edinburgh, U.K., in 2006, and the Ph.D. degree in mathematics from the University of Strathclyde, Glasgow, U.K., in 2010.

From 1987 to 1999, he was a Software Engineer in industry. Since 2010, he has been a Research Fellow with the Photonics Group, Department of Electronic and Electrical Engineering, University College London, London, U.K. His current research interests include computational modeling of novel microwave devices using liquid-crystal substrates for tunability, computational modeling of tunable optical microring resonators, and the mathematical theory of liquid crystals with a particular focus on smectic C* liquid crystals.

Sally E. Day (M'00) received the Physics degree from St. Hilda's College, Oxford University, Oxford, U.K., in 1983, and the D.Phil degree from Oxford University, Oxford, U.K., in 1988.

She spent five years with Thorn EMI, Central Research Laboratories (CRL), and Royal Signals and Radar Establishment (RSRE), Malvern, U.K., where she studied various aspects of the optical properties of liquid crystals, including nonlinear optical properties. In 1992, she joined the Electronic and Electrical Engineering Department, University College London, London, U.K., where she is currently a Senior Lecturer. Her research interests are in the application of liquid crystals in displays and nondisplay devices. These applications have included tunable micro-lenses, wavelength selective Fabry–Perot filters, the design of LCOS devices, cholesteric polarizers, large area display for architectural applications, and most recently, microwave devices and the optical design of an auto-stereoscopic display.

Dr. Day is the U.K. Director for the Society for Information Display. She was the recipient of a Royal Society University Research Fellowship in 1992 and the Cyril Hilsum Medal of the British Liquid Crystal Society in 2008.

F. Aníbal Fernández (M'88) received the B.Sc. degree in applied mathematics from the Universidad de Chile, Santiago, Chile, and the Ph.D. degree in electrical engineering from University College London, London, U.K.

In 1986, he joined the academic staff of the Department of Electronic and Electrical Engineering, University College London, where he has been dedicated to the development of mathematical and computer modeling methods. He has authored or coauthored over 180 research papers and conference presentations. He has authored one book. His research was initially applied to electromagnetic problems where he was involved with methods for the analysis of microwave and optical waveguiding systems, later to nonlinear optics, and since 1994, to the modeling of liquid-crystal devices.